https://www.sciencedirect.com/science/article/pii/S0939641117315114?via%3Dihub

DOI: https://doi.org/10.1016/j.ejpb.2018.03.013

European Journal of Pharmaceutics and Biopharmaceutics, Volume 127, July 2018, Pages 432-442

Research paper

An insight of in vitro transport of PEGylated non-ionic surfactant vesicles (NSVs) across the intestinal polarized enterocyte monolayers

Rosita Primavera[a,1], Paola Palumbo[b,1], Christian Celia[a,c], Benedetta Cinque[b], Elisabetta Carata[d], Maria Carafa[e], Donatella Paolino[f,g], Maria Grazia Cifone[b,*], Luisa Di Marzio[a,*]

[a] Department of Pharmacy, University of Chieti-Pescara "G. d'Annunzio", Chieti, Italy
[b] Depatment of Life, Health and Environmental Sciences, University of L'Aquila, L'Aquila, Italy
[c] Department of Nanomedicine, Houston Methodist Research Institute, Houston, TX 77030, USA
[d] Department of Biological and Environmental Science and Technology (Di.S.Te.B.A.), University of Salento, Lecce, Italy
[e] Department of Drug Chemistry and Technology, University of Rome "Sapienza", Rome, Italy
[f] Department of Experimental and Clinical Medicine, University of Catanzaro "Magna Graecia", Catanzaro, Italy
[g] IRC FSH-Interregional Research Center for Food Safety & Health, University of Catanzaro "Magna Graecia", Catanzaro, Italy

A B S T R A C T

PEGylated non-ionic surfactant-based vesicles (NSVs) are promising drug delivery systems for the local, oral and systemic administrations of therapeutics. The aim of this study was to test the cellular biocompatibility and transport of Nile Red-loaded NSVs (NR-NSVs) across the Caco-2-cell monolayers, which represent an in vitro model of human intestinal epithelium. The NR-NSVs assumed a spherical shape with a mean size of 140 nm, and a narrow size distribution. The NR-NSVs did not modify Caco-2 cell viability, which remained unaltered in vitro up to a concentration of 1 mM. The transport studies demonstrated that the NR-NSVs moved across the Caco-2 monolayers without affecting the transepithelial electrical resistance. These results were supported by flow cytometry analysis, which demonstrated that NR-NSVs were internalized inside the Caco-2 cells. Nanoparticle tracking and Transmission Electron Microscopy (TEM) analysis showed the presence of NR-NSVs in the basolateral side of the Caco-2 monolayers. TEM images also showed that NSVs were transported intact across the Caco-2 monolayers, thus demonstrating a predominant transcytosis mechanism of transport through endocytosis. The NSVs did not affect the integrity of the membrane barrier in vitro, and can potentially be used in clinics to increase the oral bioavailability and delivery of therapeutics.

1. Introduction

Oral drug administration is widely used in clinics to treat many diseases due to the fact that it is painless and that patients can medicate themselves which allows it to meet with a great degree of patient compliance and this, in turn, means a good degree of adherence to therapeutic regimens. Oral therapy is also cheaper than systemic therapy in the treatment of chronic diseases, and its regime is flexible and easy to manage as compared with systemic administration. Unfortunately, the physiological barriers (gastric acid pH), the poor water solubility and stability of drugs, and their biopharmaceutical features (retention, permeation and metabolism) limit the oral absorption of both hydrophilic and hydrophobic drugs [1,2]. Even though the benefits for patients are greater than the drawbacks, oral administration represents the main therapeutic option for treating chronic diseases. Physiological hurdles do exist though, and cannot be overcome using conventional medicines. In this attempt, colloidal nanoparticles were developed to deliver payloads, and modulate and target drugs to specific tissues after oral administration [3]. Specific polymeric nanoparticles, micelles and liposomes were designed to promote oral absorption, improve the bioavailability of drugs, and allow their passage through the tight junctions (TJs). These colloidal nanoparticles can resist inactivation by acid (pH 2–4) and digestive enzymes, and protect payloads from degradation following oral administration, thus modulating drug release and targeting specific tissues [4–8]. The mucus of the gastro-intestinal (GI) tract can also modify the oral delivery of colloidal nanoparticles besides their transport across the GI barrier, thus affecting the therapeutic response of the drug in various acute and chronic diseases [9–11]. Size, surface properties, and particle concentrations can all influence the transport of colloidal nanoparticles across the human mucus monolayer [9,12]. In fact, the experimental modifications of the surfaces of the colloidal nanoparticles allowed them to overcome the mucus barrier, and increased their penetration across the epithelial cells of the GI tract [3]. Polyethylene glycol (PEG), a food and drug administration (FDA)-approved hydrophilic polymer, is currently being used to overcome the monolayer mucus barrier of the GI tract due to its long hydrophilic, polyethylene-oxide chains, which decrease the uptake of nanoparticles mediated by mononuclear phagocytic system (MPS), avoid interaction between nanoparticles, and stabilize the nanoparticles in biological fluids [13,14]. Previous studies demonstrated that PEG-coated liposomes, orally administered to deliver insulin in diabetic rats, significantly increased their anti-diabetic response to insulin, and provided a sustained hypoglycemic effect in hyperglycemic rats as compared to insulin delivered using naked liposomes. The resulting data demonstrated that the PEGylated liposomes were stable at the acid pH of the GI tract, prevented the

degradation of bile salts, and interacted with the intestinal wall by adhering to the mucous layer [15]. Moreover , PEGylation facilitated the diffusion of the nanoparticles across the mucus barrier due to the effect of the interpenetration of the polymer network between the PEG chains and the mucus mesh fibers, and/or the hydrogen bonding that comes about between the ether oxygen atoms of PEG and the polysaccharide residues of glycosylated mucins [16]. The physicochemical properties of PEG such as density, molecular weight, and pending chain derivatives, can affect the diffusion of PEGylated nanoparticles through human mucus. In particular, several studies have demonstrated that the increase of PEG density and the decrease of the molecular weight of PEG increased the penetration of the nanoparticles in highly viscoelastic human mucus [17–20]. Through PEGylation, researchers can develop colloidal nanoparticles which can effectively penetrate the mucus layer and then accumulate on the surfaces of epithelial cells. Nanoparticles can move across the intestinal epithelium, and reach the blood stream by way of two different routes: (i) paracellular, and (ii) transcellular pathways. Paracellular transport involves the passive diffusion of drugs through the intercellular spaces between adjacent epithelial cells; however this is limited by the presence of the TJs [21,22]. The TJs provide a crucial structural support to the intestinal epithelium, maintain the constitutive cells in a cohesive and polarized condition and play a pivotal role in the diffusion of drugs across the intestinal monolayer [23]. The TJs, being the closely associated areas between two cells forming a virtual barrier that is impermeable to fluid, have pore sizes of 10–30 Å, and play an important role in controlling the permeability of epithelial cells. TJs also control the permeation of small hydrophilic drugs across the epithelium of the GI tract [1]. Transcellular transport includes passive diffusion, carrier-mediated transport, endocytosis, and transcytosis [24]. Passive diffusion depends on the size of nanoparticles, which limits their diffusion through cellular membranes and barriers. In order to overcome these drawbacks, the colloidal nanoparticles penetrate the cells by endocytosis [1,25]. The endocytic pathways include: (i) clathrin-mediated endocytosis, (ii) caveolae-mediated endocytosis, (iii) phagocytosis, (iv) macropinocytosis, (v) clathrin and caveolae-independent endocytosis [26,27]. In addition to using endocytic pathways, colloidal particles can also pass across the epithelial cell through transcytosis-mediated transport, which includes both endocytosis and exocytosis. The transcytosis of nanoparticles through epithelial cells involves cell-surface binding, endocytosis at the apical side of cell membranes, intracellular trafficking, and release at the basolateral side (exocytosis) of the cell membrane [1,28,29]. In a previous work, we demonstrated that NSVs of polysorbate 20, which contain repeated polyethylene oxide units similar to the PEG in the hydrophilic region of the surfactant, were stable and mucoadhesive in vitro in simulated GI fluids [30]. NSVs are stable, safe, biocompatible, cheaper than liposomes, easily stored, and increased the therapeutic efficacy of drugs in vitro and in vivo [31–33]. In this study, we investigated the physicochemical properties, such as average sizes, size distribution, zeta-potential, and morphology of the NSVs, their cytotoxicity (Caco-2 cells) and intracellular uptake, besides the transport of PEGylated NSVs through the Caco-2 cell epithelium barrier model. Caco-2 cells are basically used as in vitro models of the intestinal barrier and are approved by the FDA as a model of the human intestinal barrier. They are useful for studying the transport of drugs through the GI tract [34]. However, the intestinal epithelium consists of different types of cells, such as enterocytes, mucus-producing goblet cells, endocrine cells, and M cells. The Enterocytes make up the main population of GI cells, while goblet cells account for 10–24% [35]. Co-cultures of Caco-2 and goblet cells, i.e. HT29-MTX and HT29-H, are used to develop in vitro models of the human intestinal barrier that secretes mucus [35,36]. In order to mimic the intestinal barrier of the human GI tract, this barrier needs for the ratio between the Caco-2 and goblet cells to be optimized. In addition, there may be basic differences between the composition of the mediums and the cell culture times of the Caco-2 and goblet cells. In this attempt, we used only Caco-2 cells with the aim of obtaining a polarized epithelium model similar to that of the GI tract so that the interaction between the epithelium and PEGylated NSVs could be studied.

2. Materials and methods

2.1. Materials

Tween® 20 (Tw20), sephadex G-75, 9-(diethylamino)-5H-benzo[R] fenossazin-5H-one (Nile-Red or NR) were obtained from Acros Organics (Acros Organics BVBA, Geel, Belgium). Human epithelial colorectal adenocarcinoma cells (Caco-2 cells), trypan blue, 3-(4,5-dimethylthiazol-2-yl)-2,5-diphenyltetrazolium bromide (MTT), propidium iodide (PI), Nonidet P-40, cholesterol (CHOL) and ribonuclease (RNase) A, chlorpromazine, methyl-β-cyclodextrin and genistein were purchased from Sigma-Aldrich (Sigma Aldrich SRL, Milan, Italy). Fetal Bovine Serum (FBS), trypsin-EDTA solution 1×, Phosphate Buffer Saline (PBS), Dulbecco's Modified Eagle Medium (DMEM), glutamine, penicillin and streptomycin were purchased from Euro Clone (West York, UK). 12-BD Falcon™ cell culture inserts (pore size 0.4 μm, growth area 0.9 cm_2) were obtained by Becton Dickinson (Milan, Italy). All other products and reagents were of analytical grade.

2.2. Synthesis and purification of NSVs

PEGylated non-ionic surfactant vesicles (NSVs) were made from Tw20 and CHOL at the same molar concentration (15 mM:15 mM). NSVs were obtained using the thin-layer evaporation method as previously reported [30]. The resulting film was then hydrated by adding the HEPES buffer (10 mM, pH=7.4). NR-NVs were obtained by adding Nile Red (10 μM) to the Tw20/CHOL organic mixture before forming the surfactant film. The resulting NSVs were vortex-mixed for 5 min and then sonicated for 10 min at 60 °C using a probe sonicator (Hielscher, model UP200H, Teltow, Germany) equipped with an exponential microprobe operating at 24 kHz and amplitude of 60%, in order to obtain unilamellar suspensions. Both empty and fluorescent NSVs were then purified through Sephadex G-75 glass columns to remove the excess of un-assembled surfactants, fluorescent probe and cholesterol.

2.3. NSV characterization

2.3.1. Size and zeta potential measurements

The average size and size distribution of NSVs were measured using a Zetasizer Nano ZS (Malvern Instruments Ltd., Worcestershire, UK). Briefly, samples were diluted 1:50 (v/v) in HEPES buffer (10 mM, pH=7.4) to avoid multiscattering phenomena. The average size and size distribution were measured using photon correlation spectroscopy in line with cumulant mode fitting (Malvern Instruments Ltd., Worcestershire, UK). The instrument was equipped with a 4.5mW laser diode operating at 670 nm. Scattered photons were detected with a backscattering of 173°. A Zetasizer Nano ZS was also used to measure the zeta-potential of NSVs. The measurement was performed by using a Smoluchowski constant F (Ka) of 1.5 as a function of the electrophoretic mobility. Measurements represented the average of three batches (10 runs per measurements). Nanoparticle Tracking Analysis (NTA) was further used to evaluate the size of the NSVs. Briefly, samples were diluted with PBS (1:60, v/v) under isosmotic condition, and monitored with a NanoSight NS300 mounted with a blue (488 nm) laser (Malvern Instruments Ltd., Worcestershire, UK) using 3.1 Build 3.1.54 software for analysis. The particle size and scattered light intensity of the individual nanoparticles were acquired through a high-sensitivity sCMOS camera and extrapolated from at least five different videos. A video was taken at a rate of ≈25 frames/second. Experimental conditions of analysis are reported in Table 1.

Table 1

Set-up of Nanoparticle Tracking Analysis. The different parameters of Nanoparticle Tracking Analysis were reported. The setting of instruments allows performing the analysis and data acquisition to be performed at the best resolution

Conditions			
Temperature (°C)	28.1	28.1	28
Viscosity (cP)	0.83	0.83	0.83
Camera Type	sCMOS	sCMOS	sCMOS
Camera Level	12	12	12
Slider Shutter	1200	1200	1200
Slider Gain	146	146	146
Shutter (ms)	30	30	30
Camera Histogram Upper Limit	11,529	11,529	11,529
Camera Histogram Lower Limit	0	0	0
Frame Rate (fps)	24.98	24.98	24.98
Syringe Pump Speed (AU)	30	30	30

2.3.2. Surfactants self-assembled into NSVs
The assembling of surfactants into NSVs was evaluated using the colorimetric method as previously reported [30]. Briefly, NSVs (10 ml), previously purified through a Sephadex column, were treated with a cobalt thiocyanate solution (10 ml), and then extracted using dichloromethane (10 ml). The concentration of self-assembled surfactants was evaluated by measuring the absorbance of the organic phase after the extraction with a Cary 50 Scan spectrophotometer (Varian Inc. Corporate, Palo Alto, USA) at 620 nm, and was quantified by comparing results with those of a linear calibration curve of surfactants (0.6–10 μg/ml). The percentage of self-assembled NSVs represented the ratio of surfactants (w/w) composing the NSVs as compared to the total amount added to the NSVs during the preparation procedure.

2.3.3. Transmission electron microscopy analysis
Transmission Electron Microscopy (TEM) was carried out as previously reported [37]. Briefly, the NSVs were suitable diluted before TEM analysis to avoid aggregation of colloidal nanoparticles; the resulting suspensions were dropped onto a carbon-coated copper grid, and after 20 s of incubation the excess was removed using filter paper. The samples were then air-dried at room temperature for 10 min and negatively stained with 0.5% (v/v) uranyl acetate for 20 s. The TEM images and electron diffraction patterns were carried out at 100 KV with an electron microscopy Hitachi 7100 (Hitachi Medical System S.p.A., Milano, Italia) in order to obtain good resolution and minimal radiation damage of the NSVs.

2.4. Cell culture and treatment
2.4.1. Caco-2 cells
Caco-2 cells were used at passages 15 and 20. The Caco-2 cells were grown in the DMEM supplemented with 10% (v/v) FCS, 1% (v/v) non essential amino acid, 1mM sodium pyruvate and 2mM L-glutamine, 100 U/ml penicillin and 100 μg/ml streptomycin (complete medium), in a humidified incubator 5% CO_2, 95% air atmosphere at 37 °C. These culture conditions allowed the Caco-2 cells to be proliferative and undifferentiated [38]. The cell culture medium was replaced every 2 days until cells reached 60–70% confluence and then harvested using a trypsin-EDTA solution to detach them from the bottom of the flask.

2.4.2. Cytotoxicity studies
The cytotoxicity of the NSVs was tested using Caco-2 cells by means of (3-(4,5-dimethylthiazol-2-yl)-2,5-diphenyltetrazolium bromide) (MTT) assay and dye exclusion testing.

2.4.2.1. MTT test.
The Caco-2 cells were seeded in 96-well culture dishes (20,000 cells/cm^2) and allowed 24 h to attach themselves. The culture medium was then removed, replaced with the NSVs at different concentrations (0.25–5 mM), and incubated at various times (8, 12, 24 and 48 h). The NSVs were then removed, and 20 μl of MTT (5 mg/ml in PBS) were added to each well. After 4 h incubation, the MTT was removed and the resulting formazan crystals were dissolved with 200 μl of a dimethylsulfoxide/ethanol solution (1:1 v/v). The 96-well culture dishes were then shaken at 230 rpm (Oscillating Stirrer 722, ASAL s.r.l. Milan Italy) for 20 min. The absorbance of different samples was measured using an ELISA microplate reader (iMark Microplate Absorbance Reader) at 590 nm. The percentage of viable cells was determined according to the following equation (Eq. (1)):

$$\text{Cell viability (\%)} = (Abs_{(T)}/Abs_{(C)}) \times 100 \quad (1)$$

where $Abs_{(T)}$ is the absorbance of treated cells and $Abs_{(C)}$ is the absorbance of control (untreated) cells. The formazan concentration was proportional to the viable cell number.

2.4.2.2. Trypan blue dye exclusion test.
The Caco-2 cells at 70–80% confluence were treated with NSVs at different concentrations (0, 1, 4 mM) and incubation times (8, 12, 24, 48 h) as previously reported [39]. Briefly, the cells were detached using a solution of trypsin/EDTA, centrifuged (800g for 10 min at 4 °C), and then washed twice with PBS. The supernatant was with drawn and the resulting pellet was dissolved in a PBS. The cells were then counted using a Burker chamber and their viability was assessed by Trypan blue dye exclusion assay. The number of viable cells was calculated using the following equation (Eq. (2)):

$$\text{Cell viability (\%)} = (V_c/T_c) \times 100 \quad (2)$$

where V_c is the number of viable cells and T_c is the total number of cells (living and dead cells).

2.4.3. Cell cycle analysis
The cell-cycle analysis was carried out by staining cell DNA with propidium iodide (PI). The labeling cells were then analyzed by flow cytometry. The Caco-2 cells at 70–80% of confluence were treated with NSVs as reported for dye exclusion test (Section 2.4.2.2). After treatment, the medium was removed, the cells washed with PBS, harvested with a trypsin/EDTA solution, and finally centrifuged (800g for

10 min at 4 °C). The resulting pellet was washed in PBS, and fixed in ice-cold ethanol (70%) at 4 °C for 30 min. The fixed cells (10_6 cells/ml) were then washed twice with the ice-cold PBS, and stained with a mixture solution of propidium iodide (50 μg/ml), Nonidet-P40 (0.1% v/v), and RNase A (6 μg/10_6 cells) for 30 min in the dark at 4 °C. Cell-cycle phasedistribution was analyzed using a flow cytometry. Data from 10,000 events per sample were collected and analyzed using a FACSCalibur (Beckton Dickinson, San Jose, CA) instrument equipped with a cell-cycle analysis software (Modfit LT for Mac V3.0). The results were expressed as the percentage of cells in each phase of the cycle. Apoptotic cells were determined by their hypochromic subdiploid staining profiles, and analyzed using Cell Quest software (BD Biosciences, San Jose, CA).

2.4.4. Transepithelial electrical resistance (TEER) analysis

The Caco-2 cells were seeded at a density of 400,000 cells/insert in 12-well cell culture inserts (pore size 0.4 μm, growth area 0.9 cm_2), incubated with the complete DMEM for 16–21 days at 37 °C, 95% relative humidity, and 5% CO_2. The medium was replaced every 2 days with 1.0 ml of fresh medium in the apical (AP) chamber, and 1.5 ml in the basolateral (BL) chamber. The integrity of the cell monolayer was evaluated by transepithelial electrical resistance (TEER) using a Millicell ERS-2 system (Millipore Corporation, Bedford, MA), equipped with STX01 electrode (World Precision Instruments, Sarasota, FL), and visually checked under a light microscope. Images were acquired by an inverted light microscope (Eclipse TS 100, Nikon) at 10×and 20×magnifications.

The TEER values of each monolayer were evaluated every 2 days.

The TEER value was determined according to the following equation

(Eq. (3)):

$$TEER = (R_{Sample} - R_{Blank}) \times A_{Transwell} \quad (3)$$

where R_{Sample} was the resistance of insert with the Caco-2 cells, R_{Blank} was the resistance of no cells insert, and $A_{Transwell}$ was the membrane surface area of the transwell. Inserts with initial TEER values between 800 and 1000 Ω×cm_2 and with unbroken and polarized cell monolayers, similar to the epithelial lining of small intestine (Fig. 1), were used for the uptake and transport experiments across the Caco-2 monolayer [40,41]. Results were the average of four different experiments as duplicated. All the values were normalized according to the initial TEER value obtained for each sample.

2.4.5. Uptake and transport of NR-NSVs across the polarized enterocyte monolayers

Caco-2 cells forming a whole monolayer were incubated with complete DMEM (control), empty NSVs (1 mM) and NR-NSVs (1 mM) at different times (0–8 h). At the end of the incubation time, the medium was removed from the AP and BL chambers, and replaced with the same volume of PBS for TEER determination as reported (Section 2.4.4). The media of the AP and BL chambers were withdraw and collected for the NTA and TEM analysis; while the Caco-2 monolayer was harvested using trypsin/EDTA, centrifuged (400g for 10 min at 4 °C), washed twice with 2 ml PBS (400g for 10 min at 4 °C), and then suspended in 1 ml of PBS. In order to detect NSV uptake, the living cells were determined through trypan blue exclusion testing (check experimental details in Section 2.4.2.2), suspended at a final concentration of 10_6 cell/ml and analysed by flow cytometry. To distinguish the associated or bound vesicles from the internalized vesicles, the cells were treated with trypan blue as previously reported [27]. The fluorescent cells (20,000 cells) were analyzed in FL2 channel (λ_{exc}=488 nm and λ_{em}=625 nm) by FACSCalibur flow cytometry. The vesicle uptake monitored by Nile-Red fluorescence was shown as histogram mode on a logarithmic scale. The resulting graphs showed the percentage of fluorescent-positive cells. The fluorescence intensity of the empty NSVs taken up from Caco-2 cells was used as blank. The NSV sizes and concentrations in AP and BL were also evaluated by using the NTA analysis (check experimental details in Section 2.3.1).

2.4.6. Mechanism of the transport of PEGylated NSVs across Caco-2 cells

Caco-2 cells were incubated together with the pharmacological inhibitors of different cellular endocytosis pathways: i) chlorpromazine, ii) methyl-β-cyclodextrin and iii) genistein. The concentration of the inhibitors was dosed at sub-toxic concentrations (data not shown). Caco-2 cells were pre-incubated with chlorpromazine (10 μg/ml) and genistein (2.5 mg/ml) for 60 min at 37 °C in complete mediums; whereas methyl-β-cyclodextrin (5.6 mg/ml) was incubated for 15 min at 37 °C. The NR-NSVs (1 mM) were then added to the Caco-2 cells, and the cells were incubated for another hour at 37 °C. The Caco-2 cells incubated with chlorpromazine were washed with PBS (3 times), and then incubated with NR-NSVs for 15 min, because the effects of chlorpromazine are quickly reversible [27]. After incubation, the cells were further washed with cold PBS, harvested using trypsin/EDTA, centrifuged (400g for 10 min at 4 °C), washed twice with 2 ml PBS (400g for 10 min at 4 °C), and then suspended in PBS (1 ml). The resulting cell suspension was investigated by flow cytometry as herein reported (check experimental details in Section 2.4.5). The control was Caco-2 cells incubated with NR-NSVs (1 mM) without inhibitors.

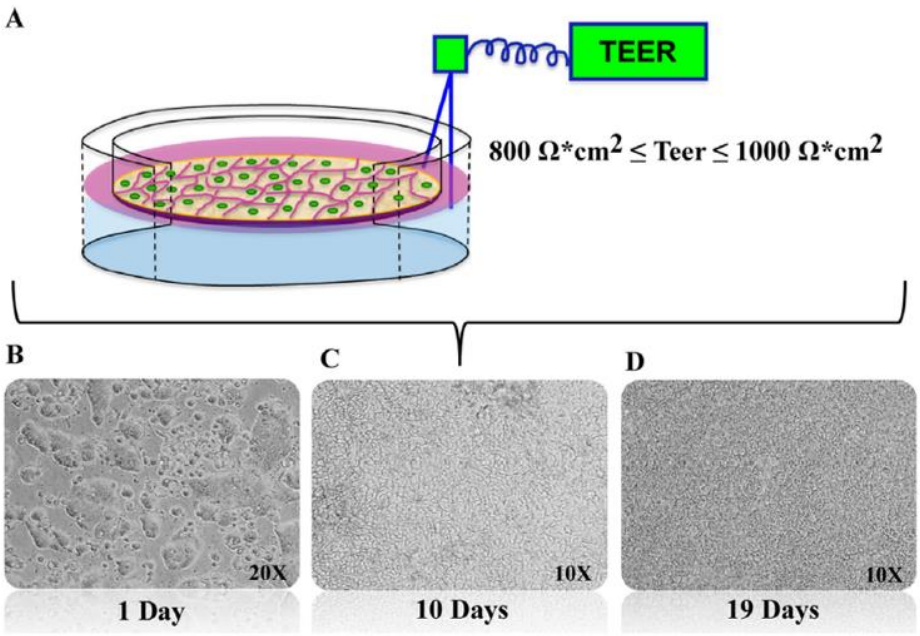

Fig. 1. Cell monolayer integrity. The cell monolayer integrity was evaluated using the transepithelial electrical resistance (TEER) and optical microscope. The cartoon shows the Caco-2-cell monolayer in transwell dishes and the values of TEER, which resulted in an intact monolayer (A). A representative optical image of Caco-2-cell monolayer, showing three independent experiments, at 1 day (B), 10 days (C), and 19 days (D) was herein reported. The magnification was 10× for Caco-2-cell monolayer incubated at 10 (C) and 19 (D) days, and 20× for Caco-2-cell monolayer incubated at 1 day (B).

2.4.7. Statistical analysis

Data are the mean of two different experiments ± standard deviation (SD) or standard error of mean (SEM) unless otherwise specified. Statistical analysis was performed using Prism 6.0 Software (GraphPad Software, Inc., San Diego, CA, U.S.A.). The Student's unpaired t test was used to compare the clusters of analysis. One or twoway ANOVA and Bonferroni post–hoc tests were used during the analysis. Values of $p < 0.05$, $p < 0.01$ and $p < 0.001$ were considered statistically significant, highly significant, and hugely significant, respectively.

3. Results and discussion

3.1. Physicochemical characterization of NSVs

The mean sizes of NSVs were determined through DLS and NTA analysis. DLS analysis showed that NR-NSVs had narrow size distributed (polydispersity index below 0.2), and had a mean size of 138 ± 0.39 nm (Fig. 2A). This data was in agreement with the NTA analysis (Fig. 2B), which demonstrated that the nanoparticles had a mean equivalent spherical size similar to that seen during DLS analysis.

These results depended on the narrow size distribution of NSVs. In fact, larger particles generated positive and negative interference in the scattered light due to their relative Brownian motion in suspension, providing a significant variation of the hydrodynamic radius obtained through DLS analysis [42]. Conversely, the NTA analysis directly measure the diffusion of single particles in a heterogeneous suspension by applying the Stokes-Einstein equation and normalizing the effect of noise due to the interference of the Brownian motion of the particles [43]. The size distribution, zeta-potential, and entrapment efficiency of the NR-NSVs were all in agreement with data previously reported [44]. The percentage of Tw20 self-assembled into the NSVs was 40.26% and 47.55% for empty- and NR-NSVs, respectively (Table S1).

NTA analysis allowed further evaluation of the particle concentration of NR-NSVs [43], which was $2.66\ e_{+13} \pm 1.24e_{+12}$ (particles/ml) (Fig. 2B). The morphology of NR-NSVs was carried out by TEM, which showed that the NSVs had a spherical and/or ellipsoidal shape, and were unilamellar (Fig. 2C). TEM data was in agreement with the DLS analysis (Fig. 2A).

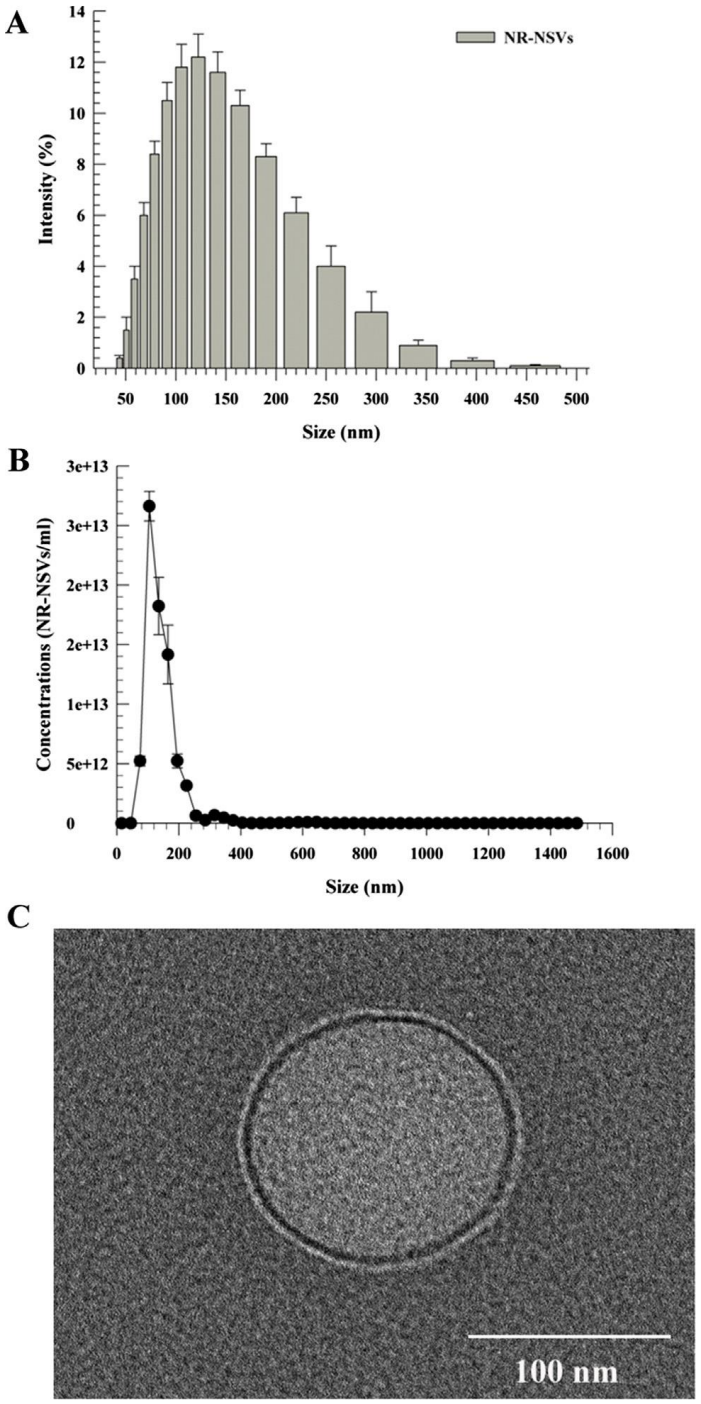

Fig. 2. Physicochemical characterization of NR-NSVs. The average sizes of NRNSVs were determined through DLS (A), NTA (B) and TEM (C) analysis. Data of DLS and NTA analysis were the mean ± S.D. of three independent experiments in triplicate, while the TEM analysis was a representative image of three independent experiments.

3.2. Cell viability of NSVs

The MTT assay demonstrated that the cell viability was time- and dose-dependent; in particular, the cell viability percentage (80–100%) was not affected by the NSV concentration in the range between 0.025 and 1.5mM at different incubation times (Fig. S1). Conversely, a significant ($p < 0.05$) degree of cell toxicity was obtained by treating Caco-2 cells with at NSVs 2.5mM (% of viable cells≈20%). Similar results were obtained using NSVs at 4 and 5 mM, respectively (Fig. S1). This effect depends on the lack of the integrity of Caco-2-cell monolayer occurring

after a toxic administration in vitro of bioactive compounds and macromolecules [45,46]. The cytotoxicity of NSVs at 1 and 4mM was also evaluated by using trypan-blue dye (Fig. 3). The results demonstrated that the percentage of living cells was ≈90% at a 1mM concentration of NSVs at different incubation times (Fig. 3). This data was similar to control (untreated cells), thus showing the lack of toxicity of NSVs. Conversely, a 4mM concentration of NSVs was significantly ($p < 0.05$) toxic to the Caco-2 cells, and less than 25% of the cells were still alive after treatment at different incubation times (Fig. 3). The significant cytotoxicity of NSVs at a 4mM concentration may have depend on the high viscosity of the resulting nanoparticle suspension, and the dehydration and clumping of the cells as previously reported for branched and linear polymeric derivatives, similar to the polyethylene oxide units of surfactants forming the NSVs [47]. The microscopic analysis of transwell inserts containing Caco-2-cell monolayer without any treatment (control) (Fig. 4A), was similar to the Caco-2-cell monolayer treated with NSVs at a 1mM concentration (Fig. 4B), and did not show any significant morphological changes. Conversely, the Caco-2-cell monolayer of samples treated with NSVs at a 4mM concentration did not form a continuous monolayer and showed different cell-free zones compared to control (Fig. 4C).

3.3. Effect of NSVs on the cell-cycle profile of Caco-2 cells

The alteration of cell-cycle progression of the Caco-2-cell monolayer treated with NSVs was evaluated at 1mM and 4mM concentrations. This was to measure the DNA content of living cells staining with PI, and was done by means of a flow cytometry The cell percentage in the different phases of their cycle was compared to control (complete DMEM) (Table 2). The results demonstrated that NSVs at 1mM concentration had no effect on the cell-cycle distribution of the Caco-2 cells at different incubation times (Fig. 5 and Table 2); whereas NSVs at a concentration of 4mM modified the cell-cycle distribution of the Caco-2 cells as compared to the control cell (Fig. 5 and Table 2) groups. In fact, the G2-phase of the Caco-2 cells decreased, while the S-phase increased at different incubation times (Fig. 5 and Table 2). The resulting data demonstrated that the NSVs were not toxic at the 1mM concentration (Fig. 5 and Table 2). In order to ascertain whether the treatment of the Caco-2 cells with 4mM was associated with the induction of apoptosis, the population of the cells in the sub-G1 was analyzed. The percentage of the apoptotic Caco-2 cells (analyzed by flow cytometry) which accumulated in the hypochromic subdiploid peak increased when the cells had been treated with 4mM of NSVs. These results demonstrated that no significant apoptosis was obtained when the Caco-2-cell monolayer was treated at a 1mM concentration (Table S2) as can be seen from the lack of cell population in the sub-G1 apoptotic peak (< 5%) (Table S2); conversely, apoptosis (< 10%) increased when Caco-2 cells were treated with NSVs at a concentration of 4mM for 8 and 12 and 24 h (Table S2).

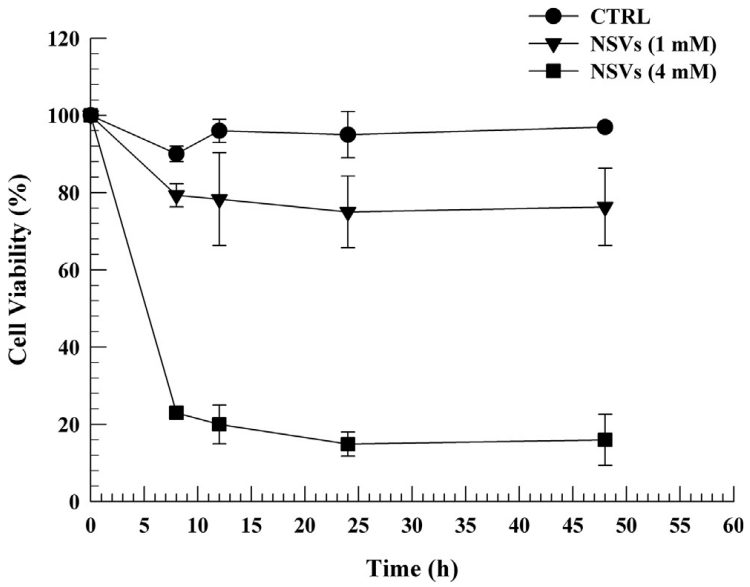

Fig. 3. Effect of NSVs on Caco-2 cells. The cytotoxic effect of NSVs (Tw20:CHOL, 15 mM:15 mM) was evaluated by Trypan blue dye exclusion assay. Data were the mean ± S.D. of five independent experiments in triplicate. Standard deviation bars if not shown were within the symbols. *$p \leq 0.05$ was considered statistically significant compared to control (CTR).

3.4. TEER analysis of Caco-2-cell monolayer treated with NSVS

Caco-2-cell monolayers were used as an in vitro model of intestinal mucosa in order to evaluate the gastrointestinal transport of hydrophilic macromolecules as previously reported [48]. The TEER values of caco-2-cell monolayers can be used to predict the opening of TJs between epithelial cells and the permeation of nanoparticles through the paracellular pathway [49,50]. The TEER values decreased significantly when nanoparticles broke the integrity of the epithelial monolayer by opening the TJs, thus showing their passage through gastrointestinal barriers via the paracellular route. In this attempt, the TEER analysis may confirm the effect of NSVs on the TJs in the Caco-2-cell monolayer. The treatment of Caco-2-cell monolayers using NR-NSVs (1 mM) did not significant ($p > 0.05$) modify the TEER values at different incubation times (Fig. 6), thus demonstrating that the integrity of the monolayer remained intact. Lin et al. demonstrated that the surface charge of nanoparticles affects the opening of TJs; in particular, the TJs are opened by positively-charged nanoparticles and are unchanged by using negatively-charged nanoparticles are used [51]. Moreover, PEGylated nanoparticles can permeate across the Caco-2 monolayer via the transcellular pathway [52]. Conversely, the NSVs did not permeate across the TJs of epithelial cells, maybe due to the presence of the –OH groups in the polyethylene oxide (PEO) chains of the surfactants. The PEO moieties decreased the adhesion of the NSVs to the Caco-2-cell monolayer, and shrank the opening of TJs, which were in contact with PEG coating of the PEGylated nanoparticles [53].

3.5. Transcellular transport

The TEER analysis demonstrated that the NSVs did not affect the integrity of the TJs of the Caco-2-cell monolayer by opening them, thus showing that they can move across whole biological membranes using different pathways. The uptake and trafficking of the NSVs through the Caco-2- cell monolayer was then evaluated by flow cytometry. The Caco-2-cell monolayers treated with NR-NSVs showed that the percentage of positive cells (Fig. 7A) and their fluorescent intensity (Fig. 7B) increased at different incubation times. These results demonstrated that the NR-NSVs were taken up inside the Caco-2-cell monolayer, thus increasing the resulting fluorescent intensity of the cells. This effect was time-dependent for the fluorescent NSVs. The Caco-2 cells treated with empty NSVs showed a flow cytometry profile that overlapped with that of cells incubated with cell culture medium (Fig. 7B). Conversely, the flow cytometry profile shifted to the right side of the graphs, thus showing an increased fluorescence of NR inside the positive Caco-2 cells (Fig. 7B). Other studies also demonstrated a transport of anionic and PEGylated nanoparticles inside Caco-2- cell monolayer by transcytosis. In fact, these nanoparticles can penetrate across the Caco-2-cell monolayers by means of lipid raft/caveolae-mediated endocytosis at the apical side of the membrane, and then leave the cell membrane by exocytosis at the basolateral side [52,54–56].

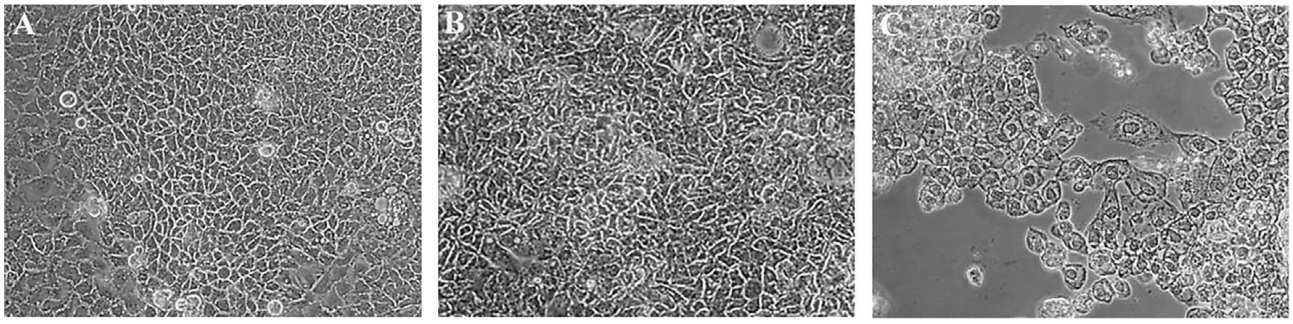

Fig. 4. Optical microscope images of an AP transwell insert with Caco-2-cell monolayer. Morphological analysis phase of Caco-2-cell monolayer treated with NSVs at 0mM (control) (A), 1mM (B), and 4mM (C) using the optical contrast microscopy. The images were a representative example of four independent experiments in triplicate. The images were acquired with a magnification of 20×.

Table 2
Cell-cycle analysis of Caco-2-cell monolayer using NSVs. The effect of NSVs on the cell cycle of Caco-2-cell monolayer was carried out using the flow cytometry analysis. The NSVs were made up from Tw20:CHOL (15 mM:15 mM). The analysis was carried out at different concentrations (0–1 mM) and incubation times (8–48 h). Data were the mean ± SEM of two independent experiments in triplicate. A value of *p≤0.05 was considered statistically significant with respect to control (CTRL) at 48 h of incubation; while #p≤0.01 was considered statistically significant with respect control (CTRL) at 48 h of incubation.

NSVs (1 mM)					NSVs (4 mM)		
Times		G0/G1	S	G2/M	G0/G1	S	G2/M
8 h							
	CTRL	55.23 ± 1.21	28.77 ± 1.61	16.0 ± 0.41	56.62 ± 0.42	29.55 ± 1.96	13.83 ± 1.54
	NSVs	52.66 ± 0.3	33.97 ± 2.07	13.37 ± 1.77	55.46 ± 3.25	35.82 ± 4.57	8.73 ± 1.32
12 h							
	CTRL	56.17 ± 6.0	29.67 ± 3.0	14.16 ± 4.0	54.0 ± 6.0	30.0 ± 3.0	13.0 ± 3.0
	NSVs	55.84 ± 1.02	29.38 ± 0.63	14.73 ± 0.39	56.39 ± 0.61	35.48 ± 1.86	8.14 ± 1.25
24 h							
	CTRL	62.03 ± 1.0	25.42 ± 6.0	12.54 ± 3.0	62.55 ± 1.97	26.06 ± 2.47	11.39 ± 0.5
	NSVs	61.06 ± 6.08	26.57 ± 9.70	11.90 ± 3.61	56.07 ± 0.03	34.67 ± 0.99	9.26 ± 1.02
48 h							
	CTRL	62.82 ± 2.0	22.51 ± 5.4	14.66 ± 3.37	64.51 ± 3.85	22.47 ± 3.36	13.01 ± 0.49
	NSVs	61.8 ± 0.8	25.2 ± 1.9	13.0 ± 1.08	53.72 ± 0.85*	37.53 ± 2.3#	6.54 ± 0.54#

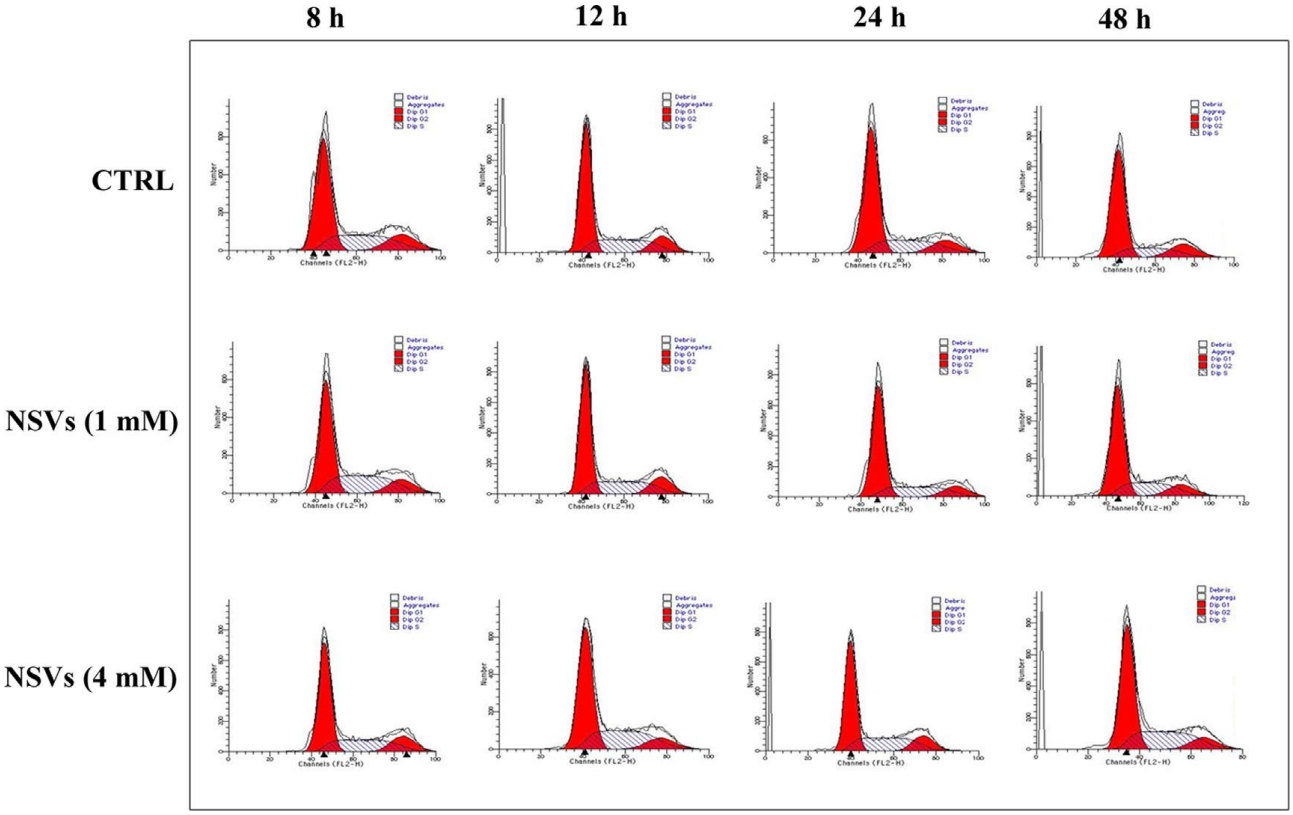

Fig. 5. Cell-cycle analysis of Caco-2 cells using flow cytometry. The Caco-2-cell monolayer were treated with NSVs (Tw20:CHOL, 15 mM: 15 mM) at two different concentrations: 1mM (A), and 4mM (B). The analysis was carried out at different incubation times (8–48 h). The acquisition was carried out using the software Modfit LT for Mac V3.0. The panels were representative analysis of five independent experiments.

Internalization experiments were performed using inhibitors of different cellular endocytosis pathways to understand whether lipid raft/caveolae-mediated endocytosis is involved in the uptake of the NRNSVs on the part of the Caco-2 cells. The use of Chlorpromazine allowed us to distinguish clathrin-dependent endocytosis from lipid raft/ caveolae-mediated endocytosis and the pinocytotic pathway [57]. A decrease of 14% was observed in the uptake of the NR-NSVs by the Caco-2 cells, when the Caco-2 cells were incubated with chlorpromazine, as compared to control (untreated cells) (Fig. 8). Conversely, methyl-β-cyclodextrin, a cyclic heptasaccharide capable of forming soluble inclusion complexes with cholesterol and hence to deplete this steroid from the lipid raft/caveolae microdomains of the plasmatic membrane [57,58], decreased the uptake of the NR-NSVs by the Caco-2 cells by a significant 70%, as compared to control (untreated cells) (Fig. 8). Polarized Caco-2 epithelial cells expressed low levels of caveolins, which are integral membrane proteins associated with caveolar membrane invaginations [59]. In fact, the uptake of the NR-NSVs by the Caco-2 cells incubated with genistein, a non-specific tyrosine kinase inhibitor which blocks caveolae-dependent endocytosis, fell by 27% [60]. These results showed that the transcytosis/endocytosis of the NRNSVs by the Caco-2 cells mainly depended on lipid raft-endocytosis, although caveolae-endocytosis can also concur to transcytosis. Lipid rafts are microdomains of plasmatic membrane, rich in cholesterol and sphingolipids, which are platforms for the proteins (ligands and receptors) involved in the mechanisms of signal transduction and membrane trafficking [61,62]. The internalization of extracellular macromolecules is mediated by lipid rafts or caveolae by either specific or non-specific interactions [63]; therefore the non-specific interactions of NR-NSVs with the cellular receptors of the lipid raft might be involved in the uptake of NR-NSVs. At the same time, the fluorescent intensity of NR-NSVs (1 mM) incubated with the Caco-2-cell monolayer in the AP and BL chambers was also quantified by using NTA analysis. Results showed that NR-NSVs moved from the AP to the BL chambers and the number of nanoparticles increased over the time (Fig. 9A). In fact, the NSV concentration was $1.09e_{+10} \pm 1.36e_{+8}$ particles/ml following 2 h of incubation and increased up to $1.52e_{+10} \pm 4.33e_{+8}$ particles/ml (4h of incubation) and $2.34e_{+10} \pm 8.25e_{+8}$ (8h of incubation), respectively (Fig. 8). Interestingly, the accumulation of NR-NSVs in the BL chamber decreased their concentration in the AP chamber (Fig. 9B) at different incubation times. Details of the dynamic process of the transport of the NR-NSVs in the Caco-2 cells have been displayed in the Supporting Information Videos. Moreover, the sizes of the NR-NSVs measured by the NTA analysis on the AP and BL samples (Fig. S2A and B) were in agreement with the DLS (Fig. 2B) and TEM (Fig. 10) analysis of NR-NSVs, respectively. The TEM analysis further showed that the NR-NSVs had similar sizes and shapes in both the AP and BL samples (Fig. 10A), and their passage across the Caco-2-cell monolayer did not affect these parameters at 4 and 8 h (Fig. 10C and D), thus demonstrated the passage of intact NR-NSVs across the intestinal epithelial model of cellular monolayer.

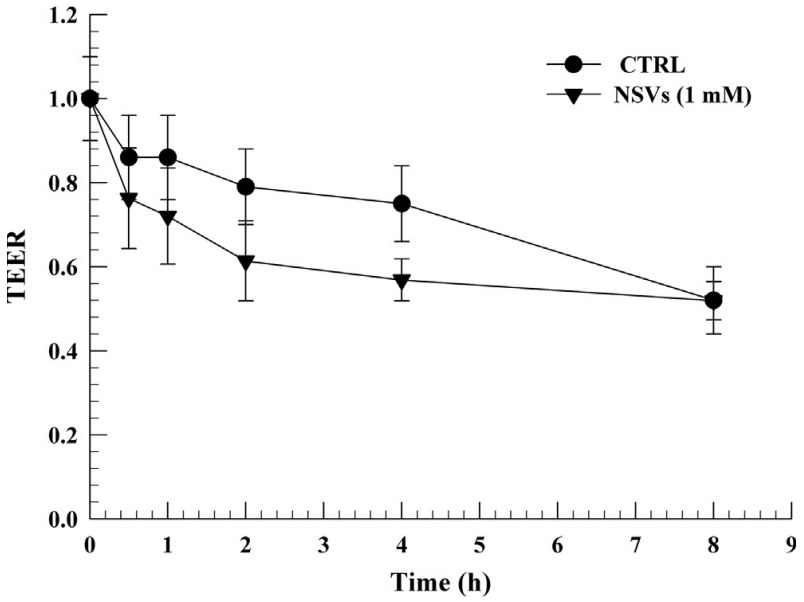

Fig. 6. Transepithelial electrical resistance determination of Caco-2-cell monolayer. The integrity of Caco-2-cell monolayer was assured by incubating Caco-2 cells with NR-NSVs (1 mM) at different incubation times (0–8 h). Untreated cells were used as control (CTRL). The NR-NSVs were made of Tw20:CHOL (15 mM:15 mM) and NR was loaded inside the NSVs during the hydration procedure. Data were the mean ± S.D. of four independent experiments in triplicate.

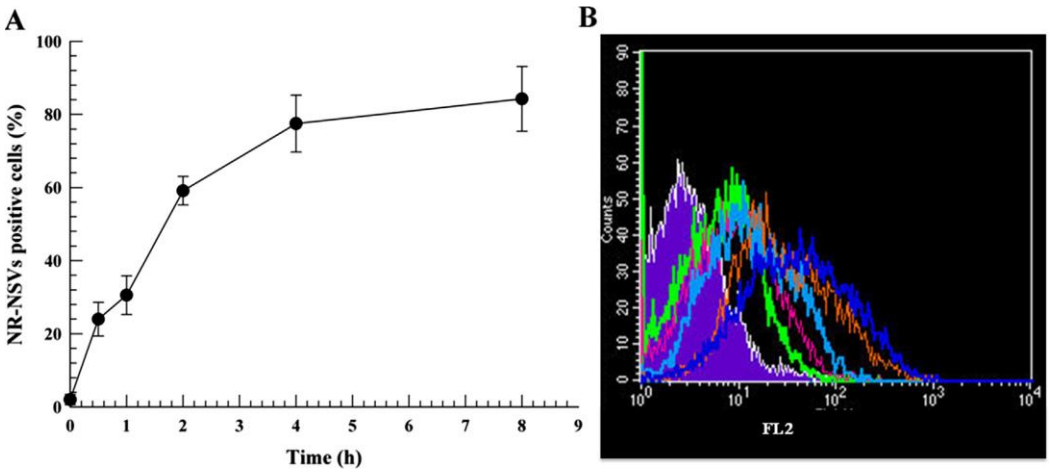

Fig. 7. Positive cell percentage of NR-NSVs in Caco-2-cell monolayer. The positive cell percentage of NR-NSVs was analyzed by flow cytometry in polarized enterocytes monolayers of Caco-2 cells at different incubation times (0–8 h). Data were the mean ± SEM of three independent experiments in triplicate. A value of *$p \leq 0.05$ was considered statistically significant for NR-NSVs at 1 h of incubation with respect to data at 0 h; #$p \leq 0.0001$ was considered statistically significant for NR-NSVs from 2 to 8 h of incubations with respect to data at 0 h (A). The flow cytometry profile of one experiment was herein reported. Key legends: purple line at 0 h of incubation time; green line at 0.5 h; fuchsia line at 1 h; turquoise line at 2 h; orange line at 4 h; and blue line at 8 h (B).

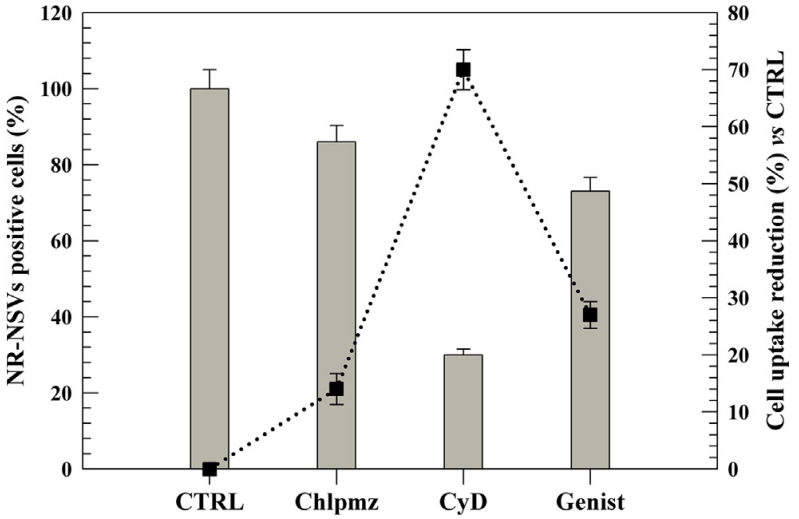

Fig. 8. Effect of the different endocytotic inhibitors on cell internalization of NR-NSVs. Cells were preincubated with chlorpromazine (chlpmz), methyl-β-cyclodextrin (CyD) and Genistein (Genist) as described in Section 2. The Caco-2 cells, with complete medium were used as control (CTRL), while the others were subsequently incubated with 1mM NR-NSVs at different as reported in Section 2. After incubation, the Caco-2 cells were washed, harvested and then analyzed by flow cytometry. Bars represent the percentage of Caco-2 positive cells after the treatment with 1mM NR-NSVs; while the full black squares represent the reduction percentage of 1mM NR-NSVs uptake from Caco-2 cells after the treatment with inhibitors. The data are shown as mean ± SEM obtained from three independent experiments. Standard deviation bars if not shown were within the symbols.

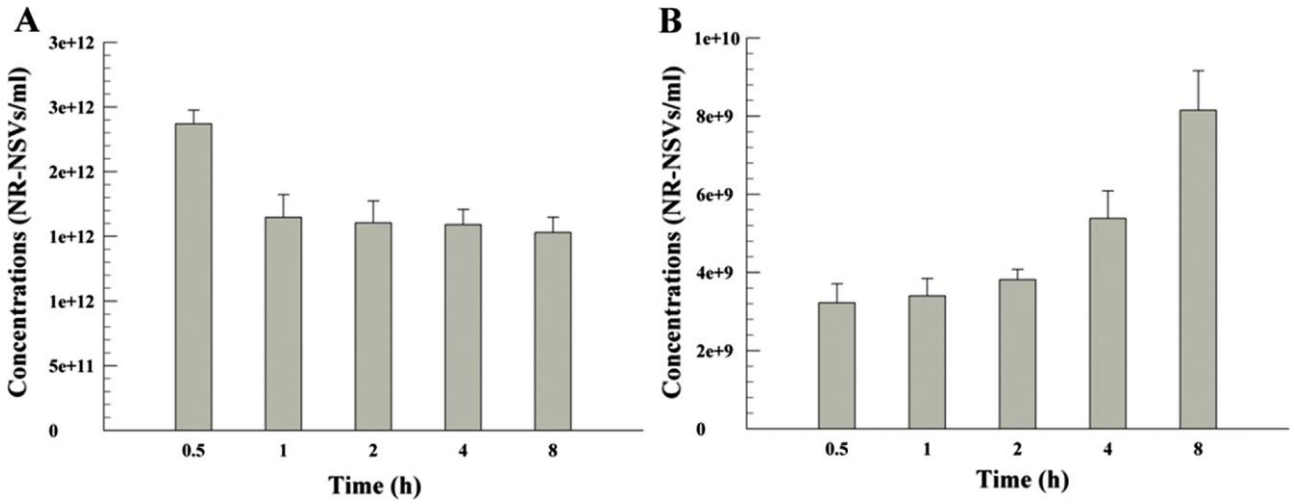

Fig. 9. Trafficking of NR-NSVs across the polarized enterocytes monolayers of Caco-2 cells. Measurements of NR-NSVs in the basolateral (A) and the apical (B) chambers of transwell dishes taken by Nanoparticle Tracking Analysis (NTA). Results were normalized removing the intensity of control (cell culture medium) from the different values. Data were the mean ± S.D. of four independent experiments in triplicate.

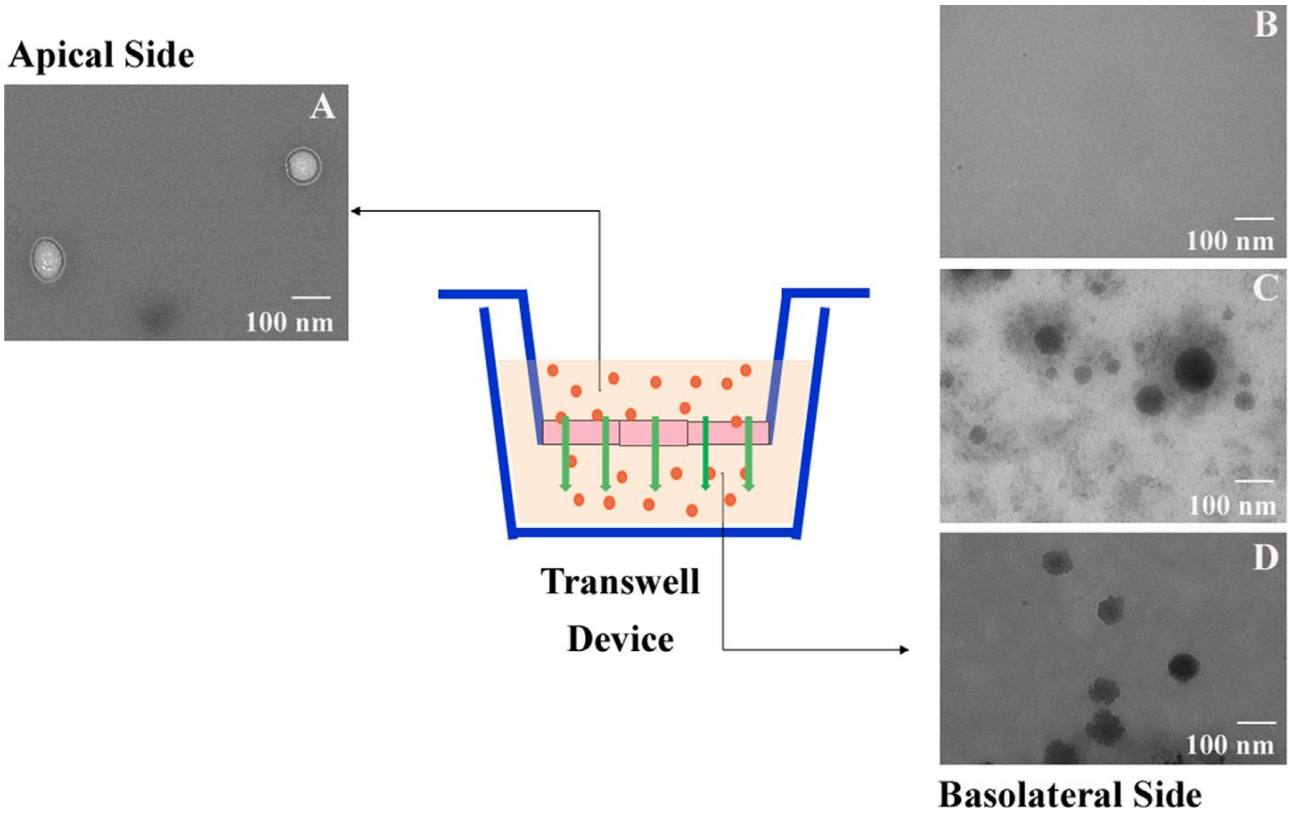

Fig. 10. TEM images of NR-NSVs moving across the Caco-2-cell monolayers. TEM images of NR-NSVs in the apical (A) or basolateral side of transwell dishes were acquired at 0 (B), 4 (C) and 8 h (D) of incubation times after the treatment of Caco-2-cell monolayers with NR-NSVs. NR-NSVs were negative stained for the acquisition of TEM images. The resulting images were a representative example of four independent experiments.

4. Conclusions

We synthetized and physicochemically characterized stable NSVs, which were safe and which had the ability to pass intact across the Caco-2-cell monolayer. The Caco-2-cell monolayer was used as a suitable in vitro model of the intestinal epithelium in order to evaluate the intracellular uptake and transport of the NSVs. Results demonstrated that the NSVs with surface properties and composition similar to that of PEGylated nanoparticles did not affect the integrity of the Caco-2-cell monolayer in vitro. In fact, PEGylation allowed the adhesion of the nanoparticles to the intestinal epithelium, and activated the transcytosis pathway. The PEO polymeric chains of surfactants affect the bioadhesive properties of the NSVs, thus introducing new strategies to increase the transport of therapeutic agents across a model of intestinal epithelial barrier. NSVs can also pass intact through the Caco-2-cell monolayer. The resulting data further demonstrated that the NSVs could be an innovative and promising nanocarrier for the potential oral administration of therapeutic agents; can improve the patient compliance and consequent adherence to a therapeutic schedule.

Conflict of interest

The authors disclose that no conflicting interests are associated with the manuscript.

Acknowledgments

Prof. Luciana Dini, from the Department of Biological and Environmental Science and Technology (Di.S.Te.B.A.), University of Salento, Lecce, Italy, for the technical support and discussion of TEM data, and Dr. Roberto Santoliquido, from the AlfatestLab, Cinisello Balsamo (MI), Italy, for the technical support and discussion of NTA analysis. The authors are also very grateful to Lynn Whitted for her expert revision of the language of this manuscript. This work was financially supported by the Inter-regional Research Center for Food Safety and Health (IRC-FSH) (grant no. PON a3_00359) and FAR-MIUR 2017, Department of Pharmacy, University of Chieti- Pescara “G. d’Annunzio”, Chieti, Italy.

Appendix A. Supplementary material

Supplementary data associated with this article can be found, in the online version, at https://doi.org/10.1016/j.ejpb.2018.03.013.

[1] E. Roger, F. Lagarce, E. Garcion, J.P. Benoit, Biopharmaceutical parameters to consider in order to alter the fate of nanocarriers after oral delivery, Nanomedicine (Lond.) 5 (2010) 287–306, http://dx.doi.org/10.2217/nnm.09.110.
[2] A.A. Date, J. Hanes, L.M. Ensign, Nanoparticles for oral delivery: design, evaluation and state-of-the-art, J. Control. Release 240 (2016) 504–526, http://dx.doi.org/10.1016/j.jconrel.2016.06.016.
[3] L.M. Ensign, R. Cone, J. Hanes, Oral drug delivery with polymeric nanoparticles: the gastrointestinal mucus barriers, Adv. Drug Deliv. Rev. 64 (2012) 557–570, http://dx.doi.org/10.1016/j.addr.2011.12.009.
[4] L.L. Chaves, S.A. Costa Lima, A.C. Vieira, L. Barreiros, M.A. Segundo, D. Ferreira, B. Sarmento, S. Reis, pH-sensitive nanoparticles for improved oral delivery of dapsone: risk assessment, design, optimization and characterization, Nanomedicine (Lond.) 12 (2017) 1975–1990, http://dx.doi.org/10.2217/nnm-2017-0105.

[5] T. Hidalgo, M. Giménez-Marqués, E. Bellido, J. Avila, M.C. Asensio, F. Salles, M.V. Lozano, M. Guillevic, R. Simón-Vázquez, A. González-Fernández, C. Serre, M.J. Alonso, P. Horcajada, Chitosan-coated mesoporous MIL-100(Fe) nanoparticles as improved bio-compatible oral nanocarriers, Sci. Rep. 7 (2017) 43099 <https://www.nature.com/articles/srep43099.pdf>.
[6] D. Desai, N. Prabhakar, V. Mamaeva, D.S. Karaman, I.A. Lähdeniemi, C. Sahlgren, J.M. Rosenholm, D.M. Toivola, Targeted modulation of cell differentiation in distinct regions of the gastrointestinal tract via oral administration of differently PEGPEI functionalized mesoporous silica nanoparticles, Int. J. Nanomed. 11 (2016) 299–313, http://dx.doi.org/10.2147/IJN.S94013.
[7] A. Makhlof, Y. Tozuka, H. Takeuchi, Design and evaluation of novel pH-sensitive chitosan nanoparticles for oral insulin delivery, Eur. J. Pharm. Sci. 42 (2011) 445–451, http://dx.doi.org/10.1016/j.ejps.2010.12.007.
[8] H. Laroui, D.S. Wilson, G. Dalmasso, K. Salaita, N. Murthy, S.V. Sitaraman, D. Merlin, Nanomedicine in GI, Am. J. Physiol. Gastrointest. Liver Physiol. 300 (2011) G371–G383, http://dx.doi.org/10.1152/ajpgi.00466.2010.
[9] A. Lechanteur, J. das Neves, B. Sarmento, The role of mucus in cell-based models used to screen mucosal drug delivery, Adv. Drug Deliv. Rev. (2017), http://dx.doi.org/10.1016/j.addr.2017.07.019.
[10] M. Dawson, D. Wirtz, J. Hanes, Enhanced viscoelasticity of human cystic fibrotic sputum correlates with increasing microheterogeneity in particle transport, J. Biol. Chem. 278 (2003) 50393–53401 <http://www.jbc.org/content/278/50/50393.full.pdf>.
[11] K. Khanvilkar, M.D. Donovan, D.R. Flanagan, Drug transfer through mucus, Adv. Drug Deliv. Rev. 48 (2001) 173–193, http://dx.doi.org/10.1016/S0169-409X(01)00115-6.
[12] D.A. Norris, P.J. Sinko, Effect of size, surface charge, and hydrophobicity on the translocation of polystyrene microspheres through gastrointestinal mucin, J. Appl. Polym. Sci. 63 (1997) 1481–1492, http://dx.doi.org/10.1002/(SICI)1097-4628(19970314)63:11<1481::AID-APP10>3.0.CO;2-5.
[13] K. Knop, R. Hoogenboom, D. Fischer, U.S. Schubert, Poly(ethylene glycol) in drug delivery: pros and cons as well as potential alternatives, Angew. Chem. Int. Ed. 49 (2010) 6288–6308 <http://onlinelibrary.wiley.com/doi/10.1002/anie.200902672/epdf>.
[14] K. Yoncheva, S. Gómez, M.A. Campanero, C. Gamazo, J.M. Irache, Bioadhesive properties of pegylated nanoparticles, Expert. Opin. Drug Deliv. 2 (2005) 205–218, http://dx.doi.org/10.1517/17425247.2.2.205.
[15] K. Iwanaga, S. Ono, K. Narioka, M. Kakemi, K. Morimoto, S. Yamashita, Y. Namba, N. Oku, Application of surface-coated liposomes for oral delivery of peptide: effects of coating the liposome's surface on the GI transit of insulin, J. Pharm. Sci. 88 (1999) 248–252, http://dx.doi.org/10.1021/js980235x.
[16] Y.Y. Wang, S.K. Lai, J.S. Suk, A. Pace, R. Cone, J. Hanes, Addressing the PEG mucoadhesivity paradox to engineer nanoparticles that “slip” through the human mucus barrier, Angew. Chem. Int. Ed. Engl. 47 (2008) 9726–9729 <http://onlinelibrary.wiley.com/doi/10.1002/anie.200803526/epdf>.
[17] Y. Cu, W.M. Saltzman, Controlled surface modification with poly(ethylene)glycol enhances diffusion of PLGA nanoparticles in human cervical mucus, Mol. Pharm. 6 (2009) 173–181 <http://pubs.acs.org/doi/abs/10.1021/mp8001254>.
[18] B.C. Tang, M. Dawson, S.K. Lai, Y.Y. Wang, J.S. Suk, M. Yang, P. Zeitlin, M.P. Boyle, J. Fu, J. Hanes, Biodegradable polymer nanoparticles that rapidly penetrate the human mucus barrier, Proc. Natl. Acad. Sci. USA 106 (2009) 19268–19273 <http://www.pnas.org/content/106/46/19268.full.pdf>.
[19] J.S. Suk, S.K. Lai, Y.Y. Wang, L.M. Ensign, P.L. Zeitlin, M.P. Boyle, J. Hanes, The penetration of fresh undiluted sputum expectorated by cystic fibrosis patients by non-adhesive polymer nanoparticles, Biomaterials 30 (2009) 2591–2597, http://dx.doi.org/10.1016/j.biomaterials.2008.12.076.
[20] S.K. Lai, D.E. O'Hanlon, S. Harrold, S.T. Man, Y.Y. Wang, R. Cone, J. Hanes, Rapid transport of large polymeric nanoparticles in fresh undiluted human mucus, Proc. Natl. Acad. Sci. USA 104 (2007) 1482–1487 <http://www.pnas.org/content/104/5/1482.full.pdf>.
[21] J.H. Hamman, G.M. Enslin, A.F. Kotzé, Oral delivery of peptide drugs: barriers and developments, BioDrugs 19 (2005) 165–177, http://dx.doi.org/10.2165/00063030-200519030-00003.
[22] J.L. Madara, Regulation of the movement of solutes across tight junctions, Annu. Rev. Physiol. 60 (1998) 143–159, http://dx.doi.org/10.1146/annurev.physiol.60.1.143.
[23] N. Schlegel, M. Meir, W.M. Heupel, B. Holthöfer, R.E. Leube, J. Waschke, Desmoglein 2-mediated adhesion is required for intestinal epithelial barrier integrity, Am. J. Physiol. Gastrointest. Liver Physiol. 298 (2010) G774–G783 <http://ajpgi.physiology.org/content/ajpgi/298/5/G774.full.pdf>.
[24] T.A. Al-Hilal, F. Alam, Y. Byun, Oral drug delivery systems using chemical conjugates or physical complexes, Adv. Drug Deliv. Rev. 65 (2013) 845–864, http://dx.doi.org/10.1016/j.addr.2012.11.002.
[25] A. Verma, F. Stellacci, Effect of surface properties on nanoparticle-cell interactions, Small 6 (2010) 12–21, http://dx.doi.org/10.1002/smll.200901158.
[26] G.J. Doherty, H.T. McMahon, Mechanisms of endocytosis, Annu. Rev. Biochem. 78 (2009) 857–902, http://dx.doi.org/10.1146/annurev.biochem.78.081307.110540.
[27] L. Di Marzio, C. Marianecci, B. Cinque, M. Nazzarri, A.M. Cimini, L. Cristiano, M.G. Cifone, F. Alhaique, M. Carafa, pH-sensitive non-phospholipid vesicle and macrophage-like cells: binding, uptake and endocytotic pathway, Biochim. Biophys. Acta 1778 (2008) 2749–2756, http://dx.doi.org/10.1016/j.bbamem.2008.07.029.
[28] S. Reis, Cellular uptake and transcytosis of lipid-based nanoparticles across the intestinal barrier: relevance for oral drug delivery, J. Colloid Interf. Sci. 463 (2016) 258–265, http://dx.doi.org/10.1016/j.jcis.2015.10.057.
[29] B. He, Z. Jia, W. Du, C. Yu, Y. Fan, W. Dai, L. Yuan, H. Zhang, X. Wang, J. Wang, The transport pathways of polymer nanoparticles in MDCK epithelial cells, Biomaterials 34 (2013) 4309–4432, http://dx.doi.org/10.1016/j.biomaterials.2013.01.100.
[30] L. Di Marzio, S. Esposito, F. Rinaldi, C. Marianecci, M. Carafa, Polysorbate 20 vesicles as oral delivery system: in vitro characterization, Colloids Surf. B: Biointerf. 104 (2013) 200–206, http://dx.doi.org/10.1016/j.colsurfb.2012.10.036.
[31] C. Marianecci, L. Di Marzio, F. Rinaldi, C. Celia, D. Paolino, F. Alhaique, S. Esposito,

M. Carafa, Niosomes from 80s to present: the state of the art, Adv. Colloid Interf. Sci. 205 (2014) 187–206, http://dx.doi.org/10.1016/j.cis.2013.11.018.
[32] S. Moghassemi, A. Hadjizadeh, Nano-niosomes as nanoscale drug delivery systems: an illustrated review, J. Control. Release 185 (2014) 22–36, http://dx.doi.org/10.1016/j.jconrel.2014.04.015.
[33] N.B. Mahale, P.D. Thakkar, R.G. Mali, D.R. Walunj, S.R. Chaudhari, Niosomes: novel sustained release nonionic stable vesicular systems–an overview, Adv. Colloid Interf. Sci. 183–184 (2012) 46–54, http://dx.doi.org/10.1016/j.cis.2012.08.002.
[34] C.A. Larregieu, L.Z. Benet, Drug discovery and regulatory considerations for improving in silico and in vitro predictions that use Caco-2 as a surrogate for human intestinal permeability measurements, AAPS J. 15 (2013) 483–497, http://dx.doi.org/10.1208/s12248-013-9456-8.
[35] C. Hilgendorf, H. Spahn-Langguth, C.G. Regardh, E. Lipka, G.L. Amidon, P. Langguth, Caco-2 versus Caco-2/HT29-MTX cocultured cell lines: permeabilities via diffusion, inside- and outside directed carrier-mediated transport, J. Pharm. Sci. 89 (2000) 63–75, http://dx.doi.org/10.1002/(SICI)15206017(200001)89:1<63::AID-JPS7>3.0.CO;2-6.
[36] A. Wikman-Larhed, P. Artursson, Co-cultures of human intestinal goblet (HT29-H) and absorptive (Caco-2) cells for studies of drug and peptide absorption, Eur. J. Pharm. Sci. 3 (1995) 171–183, http://dx.doi.org/10.1016/0928-0987(95)00007-Z.
[37] C. Marianecci, L. Di Marzio, E. Del Favero, L. Cantù, P. Brocca, V. Rondelli, F. Rinaldi, L. Dini, A. Serra, P. Decuzzi, C. Celia, D. Paolino, M. Fresta, M. Carafa, Niosomes as drug nanovectors: multiscale pH-dependent structural response, Langmuir 32 (2016) 1241–1249 <http://pubs.acs.org/doi/10.1021/acs.langmuir.5b04111>.
[38] B. Cinque, C. La Torre, F. Lombardi, P. Palumbo, M. Van der Rest, M.G. Cifone, Production conditions affect the in vitro anti-tumoral effects of a high concentration multi-strain probiotic preparation, PLoS One 11 (2016) e0163216, http://dx.doi.org/10.1371/journal.pone.0163216.
[39] P. Palumbo, G. Miconi, B. Cinque, C. La Torre, F. Lombardi, G. Zoccali, G. Orsini, P. Leocata, M. Giuliani, M.G. Cifone, In vitro evaluation of different methods of handling human liposuction aspirate and their effect on adipocytes and adipose derived stem cells, J. Cell. Physiol. 230 (2015) 1974–1981, http://dx.doi.org/10.1002/jcp.24965.
[40] H. Yasumatsu, S. Tanabe, The casein peptide Asn-Pro-Trp-Asp-Gln enforces the intestinal tight junction partly by increasing occludin expression in Caco-2 cells, Br. J. Nutr. 104 (2010) 951–956, http://dx.doi.org/10.1017/S0007114510001698.
[41] P. Artursson, J. Karlsson, Correlation between oral drug absorption in humans and apparent drug permeability coefficients in human intestinal epithelial (Caco-2) cells, Biochem. Biophys. Res. Commun. 175 (1991) 880–885, http://dx.doi.org/10.1016/0006-291X(91)91647-U.
[42] P.P. Wibroe, D. Ahmadvand, M.A. Oghabian, A. Yaghmur, S.M. Moghimi, An integrated assessment of morphology, size, and complement activation of the PEGylated liposomal doxorubicin products Doxil®, Caelyx®, DOXOrubicin, and SinaDoxosome, J. Control. Release 221 (2016) 1–8, http://dx.doi.org/10.1016/j.jconrel.2015.11.021.
[43] A. Malloy, Count, size and visualize nanoparticles, Mater. Today 14 (2011) 170–173, http://dx.doi.org/10.1016/S1369-7021(11)70089-X.
[44] R. Primavera, M. Di Francesco, A. De Cola, V. De Laurenzi, D. Paolino, M. Ciancaioni, M. Carafa, C. Celia, C. Di Ilio, A. Di Stefano, M. Fresta, M. Locatelli, L. Di Marzio, HPLC-FLD and spectrofluorometer apparatus: how to best detect fluorescent probe-loaded niosomes in biological samples, Colloids Surf. B: Biointerf. 135 (2015) 575–580, http://dx.doi.org/10.1016/j.colsurfb.2015.08.006.
[45] G. Fotakis, J.A. Timbrell, In vitro cytotoxicity assays: comparison of LDH, neutral red, MTT and protein assay in hepatoma cell lines following exposure to cadmium chloride, Toxicol. Lett. 160 (2006) 171–177, http://dx.doi.org/10.1016/j.toxlet.2005.07.001.
[46] B. Klajnert, W. Walach, M. Bryszewska, A. Dworak, D. Shcharbin, Cytotoxicity, haematotoxicity and genotoxicity of high molecular mass arborescent polyoxyethylene polymers with polyglycidol-block-containing shells, Cell Biol. Int. 30 (2006) 248–252, http://dx.doi.org/10.1016/j.cellbi.2005.10.026.
[47] R.K. Kainthan, J. Janzen, E. Levin, D.V. Devine, D.E. Brooks, Biocompatibility testing of branched and linear polyglycidol, Biomacromolecules 7 (2006) 703–709 <http://pubs.acs.org/doi/abs/10.1021/bm0504882>.
[48] I.J. Hidalgo, T.J. Raub, R.T. Borchardt, Characterization of the human colon carcinoma cell line (Caco-2) as a model system for intestinal epithelial permeability, Gastroenterology 96 (1989) 736–749, http://dx.doi.org/10.1016/S0016-5085(89)80072-1.
[49] S.M. van der Merwe, J.C. Verhoef, J.H. Verheijden, A.F. Kotzé, H.E. Junginger, Trimethylated chitosan as polymeric absorption enhancer for improved peroral delivery of peptide drugs, Eur. J. Pharm. Biopharm. 58 (2004) 225–235, http://dx.doi.org/10.1016/j.ejpb.2004.03.023.
[50] S. Yamashita, T. Furubayashi, M. Kataoka, T. Sakane, H. Sezaki, H. Tokuda, R. Primavera et al. *European Journal of Pharmaceutics and Biopharmaceutics 127 (2018) 432–442* 441
Optimized conditions for prediction of intestinal drug permeability using Caco-2 cells, Eur. J. Pharm. Sci. 10 (2000) 195–204, http://dx.doi.org/10.1016/S0928-0987(00)00076-2.
[51] Y.H. Lin, F.L. Mi, C.T. Chen, W.C. Chang, S.F. Peng, H.F. Liang, H.W. Sung, Preparation and characterization of nanoparticles shelled with chitosan for oral insulin delivery, Biomacromolecules 8 (2007) 146–152 <ttp://pubs.acs.org/doi/abs/10.1021/bm0607776>.
[52] Q. Song, X. Wang, Q. Hu, M. Huang, L. Yao, H. Qi, Y. Qiu, X. Jiang, J. Chen, H. Chen, X. Gao, Cellular internalization pathway and transcellular transport of pegylated polyester nanoparticles in Caco-2 cells, Int. J. Pharm. 445 (2013) 58–68, http://dx.doi.org/10.1016/j.ijpharm.2013.01.060.
[53] V. Uskoković, P.P. Lee, L.A. Walsh, K.E. Fischer, T.A. Desai, PEGylated silicon nanowire coated silica microparticles for drug delivery across intestinal epithelium, Biomaterials 33 (2012) 1663–1667, http://dx.doi.org/10.1016/j.biomaterials.2011.11.010.
[54] G. Sahay, J.O. Kim, A.V. Kabanov, T.K. Bronich, The exploitation of differential endocytic pathways in normal and tumor cells in the selective targeting of nanoparticulate

chemotherapeutic agents, Biomaterials 31 (2010) 923–933, http://dx.doi.org/10.1016/j.biomaterials.2009.09.101.
[55] L.W. Zhang, N.A. Monteiro-Riviere, Mechanisms of quantum dot nanoparticle cellular uptake, Toxicol. Sci. 110 (2009) 138–155, http://dx.doi.org/10.1093/toxsci/kfp087.
[56] Y.H. Sang, P.T. Gwan, Biodegradable nanoparticles containing protein-fatty acid complexes for oral delivery of salmon calcitonin, J. Pharm. Sci. 93 (2004) 488–495, http://dx.doi.org/10.1002/jps.10573.
[57] A.I. Ivanov, Pharmacological inhibition of endocytic pathways: is it specific enough to be useful? Methods Mol. Biol. 440 (2008) 15–33, http://dx.doi.org/10.1007/978-1-59745-178-92.
[58] B. He, Z. Jia, W. Du, C. Yu, Y. Fan, W. Dai, L. Yuan, H. Zhang, X. Wang, J. Wang, X. Zhang, Q. Zhang, The transport pathways of polymer nanoparticles in MDCK epithelial cells, Biomaterials 34 (2013) 4309–4326, http://dx.doi.org/10.1016/j.biomaterials.2013.01.100.
[59] P.A. Orlandi, P.H. Fishman, Filipin-dependent inhibition of cholera toxin: evidence for toxin internalization and activation through caveolae-like domains, J. Cell Biol. 141 (1998) 905–915, http://dx.doi.org/10.1083/jcb.141.4.905.
[60] S.R. Hubbard, J.H. Till, Protein tyrosine kinase structure and function, Annu. Rev. Biochem. 69 (2000) 373–398, http://dx.doi.org/10.1146/annurev.biochem.69.1.373.
[61] P. Lajoie, I.R. Nabi, Regulation of raft-dependent endocytosis, J. Cell Mol. Med. 11 (2007) 644–653, http://dx.doi.org/10.1111/j.1582-4934.2007.00083.x.
[62] I.R. Nadi, P.U. Le, Caveolar/raft-dependent endocytosis, J. Cell Biol. 161 (2003) 673–677, http://dx.doi.org/10.1083/jcb.200302028.
[63] L. Pelkmans, A. Helenius, Endocytosis via caveolae, Traffic 3 (2002) 311–320, http://dx.doi.org/10.1034/j.1600-0854.2002.30501.x.